Electronic Supporting Information
for

A Deeper Look Into The Photocycloreversion of a Yellow Diarylethene Photoswitch: Why Is It So Fast?

Arkadiusz Jarota[a], Ewa Pastorczak[b], Halina Abramczyk[a]

[a]*Institute of Applied Radiation Chemistry, Lodz University of Technology, Wróblewskiego 15, 93-590 Łódź, Poland*
[b]*Institute of Physics, Lodz University of Technology, ul. Wólczańska 219 90-924, Łódź, Poland*

1. Polarization dependence of ΔA signal probed at 440 nm.

When the DMT is probed at 440 nm (Fig. S1) and polarizations between the pump and probe beams are parallel or perpendicular to each other, apart from the long-lasting permanent ΔA signal, the short-lived component appears.

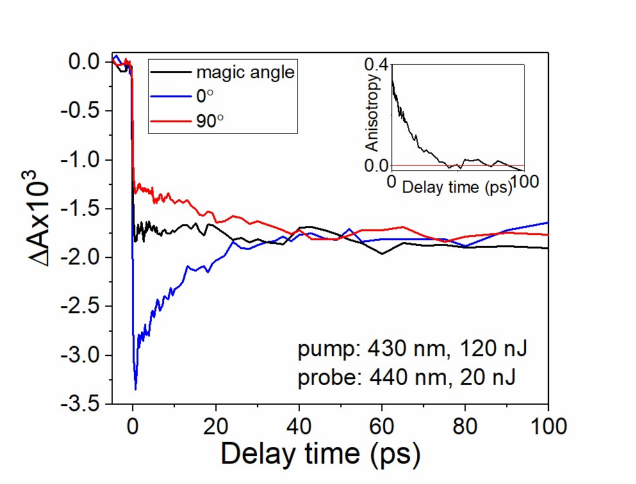

Fig. S1 The real-time trace of ΔA of PSS monitored at 440 nm following a 430 nm excitation at various relative polarizations of the pump with respect to the probe - blue line: parallel, red line: 90°, black line: magic angle.

This component is not present in the real-time trace of ΔA signal recorded at a magic angle between pump and probe at which the orientational dynamics do not impact the ΔA signal. It means that the short-lived component must represent orientational dynamics occurring upon excitation. From parallel $\Delta A_{\parallel}$ and perpendicular $\Delta A_{\perp}$ real-time traces of ΔA signal we can calculate time-resolved anisotropy changes according to eq. S1:

$$r(\lambda,t) = \frac{\Delta A_{\parallel}(\lambda,t) - \Delta A_{\perp}(\lambda,t)}{\Delta A_{\parallel}(\lambda,t) + 2\Delta A_{\perp}(\lambda,t)} \qquad (S1)$$

The calculated anisotropy is shown in the inset of Fig. 4 and features single-exponential decay with a time constant of 14.4 ± 0.6 ps and represents orientational decay time. The 14.4 ± 0.6 ps time constant is distinctly longer than that of S_1 lifetime (600 ± 40 fs) suggesting that the orientational dynamics is much longer than both relaxation processes occurring from S_1 state: $S_1 \rightarrow S_0$ nonradiative relaxation in CRI and the ring-opening reaction.

2. Electronic excitations of CRI

Table 1. Excitation energies and the oscillator strengths of the first 10 electronically excited singlet states of the closed ring isomer of DMT calculated at TD-DFT (PBE0-D3/def2-SVP) level. The NTO HOMO and LUMO of DMT closed isomer are also shown.

Excitation energy (eV)	Excitation energy (nm)	Oscillator strength	
2.90	**427**	**0.09**	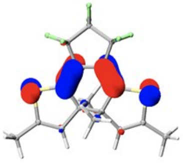 **HOMO** 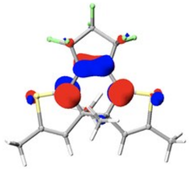 **LUMO**
3.99	310	0.03	
4.64	267	0.03	
4.66	266	0.04	
4.89	253	0.01	
5.16	240	0.05	
5.21	238	0.06	
5.58	222	0.01	
5.78	214	0.01	
5.86	212	0.00	

3. Energy gaps between the ground state of DMT and S_2 and S_3 excited states.

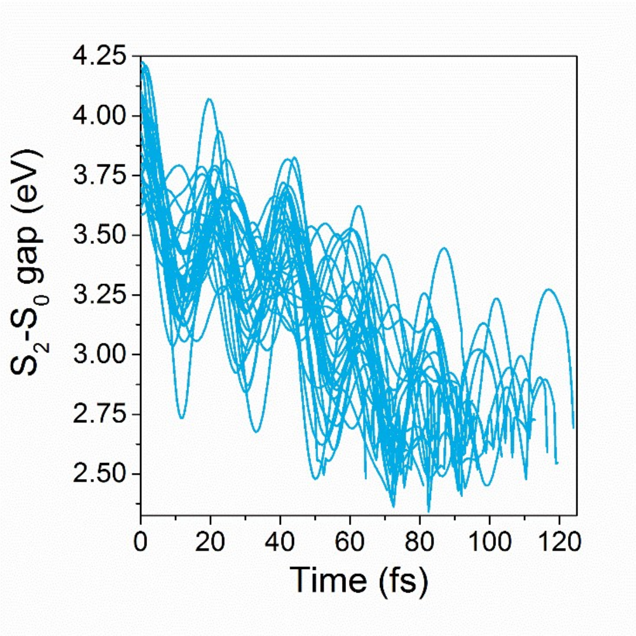

Fig. S2 The energy gap between the ground state of DMT and S2 excited state The energy gap between the ground state of DMT and S2 excited state.

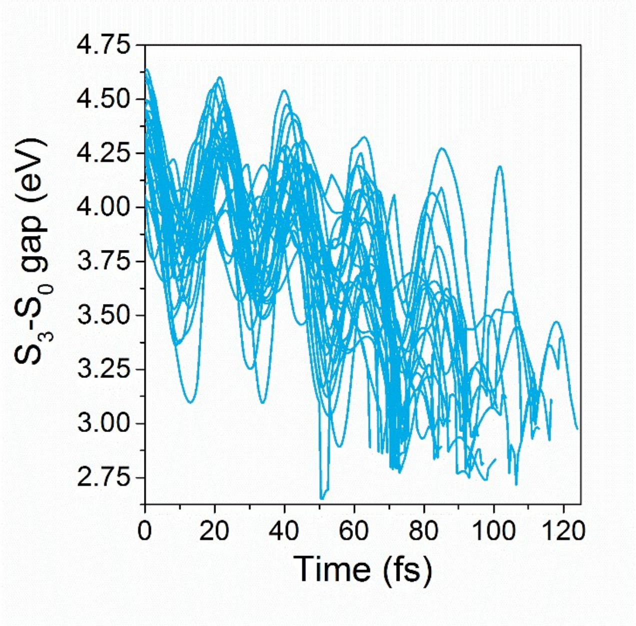

Fig. S3. The energy gap between the ground state of DMT and S_3 excited state in each of the trajectories.

4. The vibrational modes that can drive the DMT molecule from the Franck-Condon region towards CI.

To investigate vibrational modes able to drive DMT molecule from the Franck-Condon region the vibrational spectrum of DMT in the ground state has been calculated at PBE0-

D3(BJ)/def2-SVP level. As DMT nearby CI is characterized by open-like geometry the substantial change of reactive C-C bond length during the vibration is a criterion for the modes that can drive DMT molecule towards CI. In Fig. S4 several of these vibrations are shown together with atom displacement vectors.

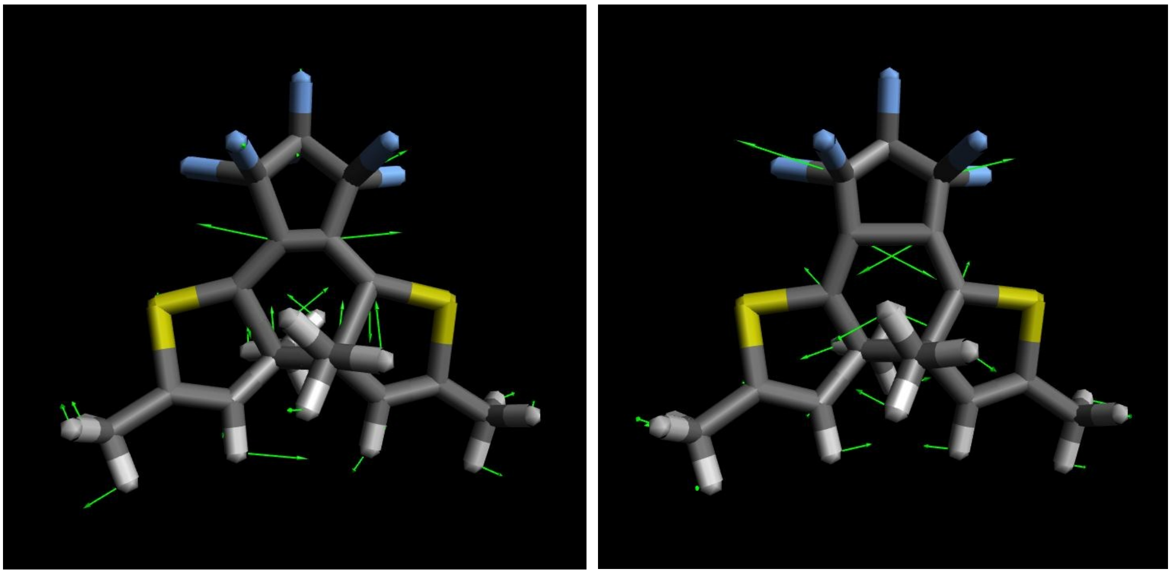

1248 cm^{-1} (48)

1404 cm^{-1} (52)

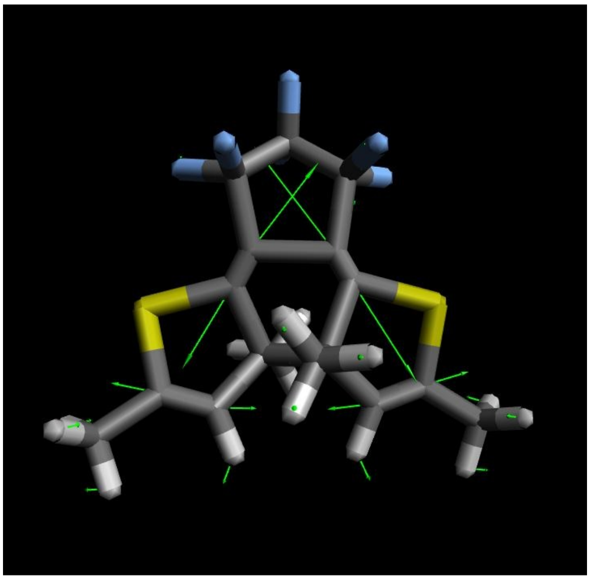

1700 cm^{-1} (660)

Fig. S4 Vibrational modes of DMT that can potentially drive the molecule towards the CI. The values in brackets indicate relative Raman activity.

5. The ground state minimum of CRI

C	-0.4156620000	-1.4118910000	0.1962960000
S	-0.6946090000	-3.1264110000	0.0900890000
C	-2.4534610000	-2.8686510000	-0.0684830000
C	-2.8134030000	-1.5861700000	0.0640390000
C	-1.7092290000	-0.6306250000	0.4304440000
C	-3.3099600000	-4.0618300000	-0.3082300000
H	-3.8575640000	-1.2673670000	0.0194000000
C	0.7492630000	-0.7402350000	0.1088310000
C	2.1518840000	-1.2600810000	0.0357010000
C	0.7638620000	0.7167140000	0.1047870000
C	2.9877110000	-0.0001020000	-0.3243090000
C	2.1736680000	1.1850060000	0.2598770000
F	2.3199970000	-2.2347600000	-0.8748850000
F	2.5800850000	-1.7443240000	1.2216180000
F	4.2328200000	-0.0567080000	0.1438380000
F	3.0243630000	0.1281660000	-1.6599650000
F	2.5214250000	1.3431150000	1.5573160000
F	2.4401290000	2.3364840000	-0.3748100000
C	-1.6629300000	0.6685350000	-0.4069370000
C	-0.3688880000	1.4172750000	-0.0917870000
C	-1.6616780000	0.3609820000	-1.9221170000
H	-1.5488780000	1.2970310000	-2.4866760000
H	-2.6070360000	-0.1170960000	-2.2172580000
H	-0.8341730000	-0.3134590000	-2.1872490000
C	-1.8016310000	-0.3248450000	1.9423780000

H	-2.7499710000	0.1813970000	2.1744320000
H	-0.9740110000	0.3238660000	2.2647440000
H	-1.7556720000	-1.2643270000	2.5106390000
H	-4.3646060000	-3.7667740000	-0.3958340000
H	-3.2193740000	-4.7856490000	0.5178710000
H	-3.0138390000	-4.5836230000	-1.2323630000
S	-0.6023660000	3.1436790000	-0.0823300000
C	-2.3739960000	2.9343280000	-0.0037600000
C	-2.7614030000	1.6580500000	-0.1197510000
C	-3.2102040000	4.1549230000	0.1564160000
H	-4.2755140000	3.8890910000	0.1956770000
H	-2.9493070000	4.6962150000	1.0799730000
H	-3.0570480000	4.8516360000	-0.6836600000
H	-3.8144240000	1.3667180000	-0.1222130000

6. The exemplary structure in the vicinity of CI shown in Fig. 4.

C	-0.5588682900	-1.3912714600	0.2031781100
S	-0.6857515900	-3.0319543400	-0.2794958100
C	-2.2881123800	-2.9432057100	-0.0280568200
C	-2.8865932700	-1.7292621900	0.4891919500
C	-1.6661796200	-0.7020748200	0.6745862800
C	-3.1474739300	-4.1733837900	-0.2675908700
H	-3.8498235500	-1.5965517200	0.7704490000
C	0.7287081100	-0.7208300000	0.0495251600
C	2.1763588400	-1.3140513700	0.1343013400
C	0.7323312500	0.7283935500	0.0030904100

C	2.9565266400	-0.0359483600	-0.2809744100
C	2.0943486300	1.1934169000	0.1497382600
F	2.3153807500	-2.2678777100	-0.8423386200
F	2.4588706400	-1.8669332100	1.2926514200
F	4.1501468000	0.0304583900	0.2860979700
F	3.1123209100	0.0842157500	-1.6038640300
F	2.4268541000	1.4954585200	1.4602413300
F	2.4228035500	2.2277044600	-0.5965973500
C	-1.7171203700	0.8128576000	-0.6378839900
C	-0.3833379300	1.3894004100	-0.2059313000
C	-1.7153997200	-0.0368146500	-1.9874900500
H	-1.6703065700	0.7582336100	-2.8275838800
H	-2.7502584300	-0.5670486500	-2.1263493600
H	-0.9351477400	-0.6873884500	-2.0920895500
C	-1.8728539100	0.1185649400	1.9432933500
H	-2.9020886800	0.5565639300	2.0609218800
H	-1.3513122600	1.2138114900	1.9026163100
H	-1.9255122800	-0.5507505000	2.8296556500
H	-4.2438876700	-3.9937704400	-0.0787888200
H	-2.9918135300	-5.0494944000	0.5477900500
H	-3.0005533300	-4.5988759400	-1.2649072500
S	-0.6062634500	2.9683634500	0.3445739100
C	-2.2654188100	3.1189095400	-0.1550419600
C	-2.6509246300	1.8330530500	-0.5878817400
C	-3.0376820200	4.2511303100	0.2150455500

H	-4.1701846300	3.9579935100	0.2645231200
H	-2.6964901600	4.5181710700	1.2909259800
H	-3.0054496300	5.2139248600	-0.3205076800
H	-3.5780282400	1.6415801600	-1.1258057000

7. Computational details

The quantum dynamics simulation was performed using the Gaussian09[1] software paired with Newton-X[2]. At PBE0-D3[3]/def2-SVP[4] level the structure of the CRI was optimized and normal modes were generated. Using the uncorrelated quantum harmonic oscillator distribution model, 29 trajectories were initiated in S_1 state and TD-DFT(PBE0-D3)/def2-SVP dynamics study involving four electronic states (S_0, S_1, S_2 and S_3) was performed using a 0.5 fs time step. To account for nonadiabatic effects, the surface hopping method employing Tully's fewest switches algorithm[5] was used. Only nonadiabatic couplings between states S_1. S_2 and S_3 were computed due to the unreliability of TD-DFT couplings for the ground state.[6] No surface hops appeared throughout the simulation. Trajectories were analyzed using VMD software, up to the gap value of 0.1 eV, before the CI is reached, according to recommendations of Barbatti[7] and Prlj[8].

8. Experimental set-up

Transient absorption (TA) measurements were performed employing femtosecond laser set-up. In this set-up Ti:sapphire oscillator (Tsunami, Spectra-Physics, 82 MHz, 800 nm, pulse duration < 100 fs) is pumped by diode laser (Millennia Pro, Spectra-Physics, 532 nm, 5 W) and amplified using regenerative amplifier (Spitfire ACE, Spectra-Physics, 1 kHz, output power: 4 W). The output from the amplifier is used to pump two optical parametric amplifiers (OPA) (Topas Prime, Light Conversion). The pulse duration in the sample position was 150 fs as measured by the cross-correlation method. The pump and probe pulse energies in TA experiments were set to be ~120 nJ and 20 nJ, respectively. The DMT solution in the PSS for TA experiments has been prepared by dissolving a powder of ORI in hexane in a concentration of 1.52 mM and its further irradiation using the output from OPA (300 nm, 15 μJ) performed until no spectral changes were detected. During TA measurements the solution was circulated in a flow cell of 630 μm path length using a peristaltic pump (Gilson, Minipulse 3) to assure that the sample is refreshed between laser shots.

9. Determination of time constant of internal conversion τ_{IC} and ring opening τ_o

The markedly short time (below 200 fs) that it takes for the molecule in the simulation to relax from FC state to CI, points to the following interpretation of the results shown in Fig. 3: the probing at wavelengths 700 and 750 nm (possibly corresponding to the $S_1 \rightarrow S_3$ excitation, see Table 1) with time constants 340 ± 20 fs and 190 ± 10 fs, respectively, illustrates the first part of the relaxation process, i.e. the molecule traveling from FC to CI, while probing at 595 nm encompasses the full relaxation until the molecule reaches the ground state of ORI or CRI with a time constant τ_{tot}=590 fs. Assuming the shortest measured time (190 fs) as the time constant of the FC to CI relaxation, τ_{CI}, in the absence of competing processes, one can estimate the time constant of the relaxation from CI to either the S_0 of ORI or CRI as $\tau_1=\tau_{tot}-\tau_{CI}$. Then, the kinetics occurring at CI can be described by equation (1):

$$\frac{1}{\tau_1}=\frac{1}{\tau_{IC}}+\frac{1}{\tau_o} \quad (1)$$

where τ_{IC} is the time constant of IC, and τ_o represents the time constant of cycloreversion reaction. In a separate experiment, we have measured the quantum yield of the ring opening φ_o upon illumination by femtosecond pulses in our set-up (100 fs, 430 nm) to be 0.7. Using this value and the relationship between φ_o and rate constants of internal conversion k_{IC} and ring opening k_o (2) τ_o and τ_{IC} are calculated to be 1 ps and 430 fs.

$$\varphi_o=\frac{k_o}{k_o+k_{IC}}=\frac{\frac{1}{\tau_o}}{\frac{1}{\tau_o}+\frac{1}{\tau_{ic}}}=\frac{\tau_1}{\tau_0} \quad (2)$$

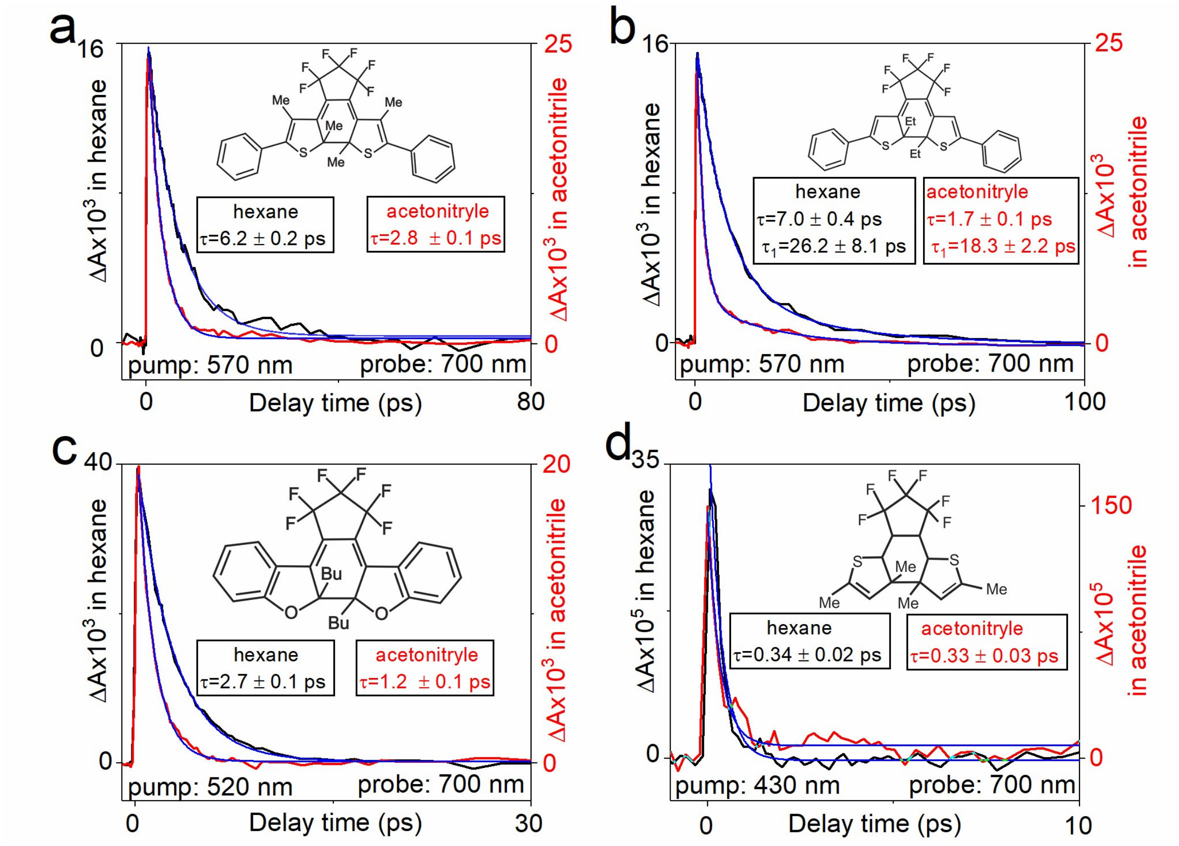

Fig. S5. Transient absorption signals of PSSs of (a) 1,2-Bis(2,4-dimethyl-5-phenyl-3-thienyl)hexafluorocyclopentene (DMP, c=0.8 mM), (b) 1,2-bis(2-ethyl-5-phenyl-3thienyl)perfluorocyclopentene (DET, 1.7 mM) , (c) 1,2-Bis(2-butyl-1-benzofuran-3-yl)hexafluorocyclopentene (DBU, c=1.6 mM) , (d) 1,2-bis(3,5-dimethylthiophen-2-yl)hexafluorocyclopentene (DMT, c=1.6 mM). The PSSs have been prepared by the same procedure as described for DMT in the experimental section (section 7 of ESI). The pump and probe pulse energies were set to 140 nJ and 20 nJ in each case, cell path length was 630 μm. The blue lines are single or double exponential fittings of the ΔA signals.

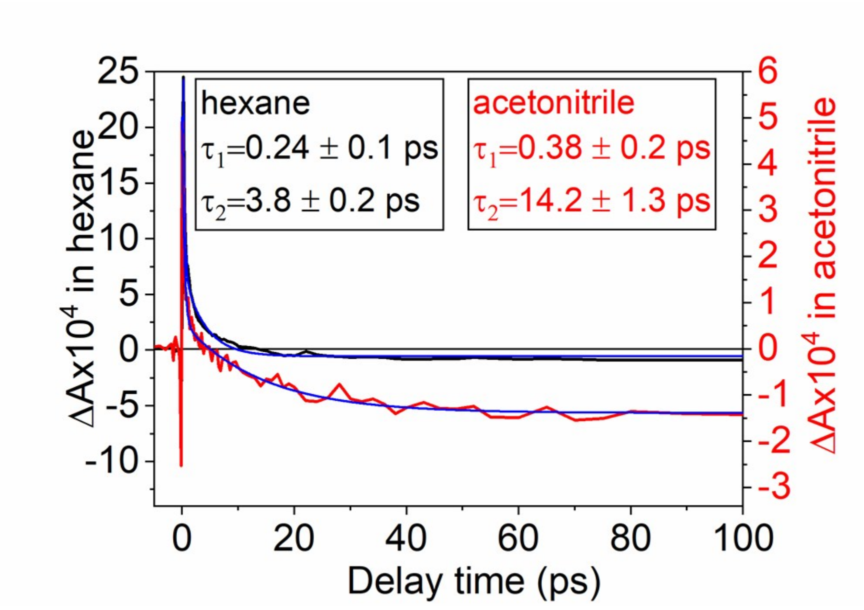

Fig. S6 Time-traces of ΔA signal of DMT in PSS monitored at 500 nm. The blue lines are single or double exponential fittings of the ΔA signals. In both cases, the ΔA signal reaches constant negative value because a certain portion of CRI molecules is permanently converted into ORI.

10. References

1 M. J. Frisch, G. W. Trucks, H. B. Schlegel, G. E. Scuseria, M. A. Robb, J. R. Cheeseman, G. Scalmani, V. Barone, B. Mennucci, G. A. Petersson, H. Nakatsuji, M. Caricato, X. Li, H. P. Hratchian, A. F. Izmaylov, J. Bloino, G. Zheng, J. L. Sonnenberg, M. Hada, M. Ehara, K. Toyota, R. Fukuda, J. Hasegawa, M. Ishida, T. Nakajima, Y. Honda, O. Kitao, H. Nakai, T. Vreven, J. A. Montgomery, J. E. Peralta, F. Ogliaro, M. Bearpark, J. J. Heyd, E. Brothers, K. N. Kudin, V. N. Staroverov, R. Kobayashi, J. Normand, K. Raghavachari, A. Rendell, J. C. Burant, S. S. Iyengar, J. Tomasi, M. Cossi, N. Rega, J. M. Millam, M. Klene, J. E. Knox, J. B. Cross, V. Bakken, C. Adamo, J. Jaramillo, R. Gomperts, R. E. Stratmann, O. Yazyev, A. J. Austin, R. Cammi, C. Pomelli, J. W. Ochterski, R. L. Martin, K. Morokuma, V. G. Zakrzewski, G. A. Voth, P. Salvador, J. J. Dannenberg, S. Dapprich, A. D. Daniels, Farkas, J. B. Foresman, J. V. Ortiz, J. Cioslowski and D. J. Fox, 2009.

2 Barbatti, M., Granucci, G., Ruckenbauer, M., Plasser, F., R. Crespo-Otero, Pittner, J., Persico, M. and Lischka, H., 2016.

3 C. Adamo and V. Barone, *J. Chem. Phys.*, 1999, **110**, 6158–6170.

4 A. Schäfer, H. Horn and R. Ahlrichs, *J. Chem. Phys.*, 1992, **97**, 2571–2577.

5 J. C. Tully, *J. Chem. Phys.*, 1990, **93**, 1061–1071.

6 M. Barbatti, *WIREs Computational Molecular Science*, 2011, **1**, 620–633.

7 M. Barbatti and R. Crespo-Otero, in *Density-Functional Methods for Excited States*, eds. N. Ferré, M. Filatov and M. Huix-Rotllant, Springer International Publishing, Cham, 2016, pp. 415–444.

8 A. Prlj, N. Došlić and C. Corminboeuf, *Phys. Chem. Chem. Phys.*, 2016, **18**, 11606–11609.